ACS Photonics

pubs.acs.org/journal/apchd5

Article

# All-Optical Switching of Silicon Nanobeam Cavities with an Ultra-compact Heater Utilizing the Photothermal Effect

Penghui Dong, Long Zhang, Daoxin Dai, and Yaocheng Shi*

Cite This: https://doi.org/10.1021/acsphotonics.1c01364

Read Online

ACCESS | Metrics & More | Article Recommendations

**ABSTRACT:** Strong light absorption by a metal-on-silicon hybrid waveguide structure can realize efficient photothermal conversion at a microscale. Based on the photothermal effect, an all-optical switch with an ultra-high tuning efficiency is experimentally demonstrated based on a suspended photonic crystal nanobeam cavity integrated with an ultra-compact metal optical heater. The measurement results exhibit a high photothermal efficiency of 15.52 nm/mW. The rising and falling times of all-optical switching are ∼6.8 and ∼1.6 μs, respectively. Moreover, the heater has only an ultra-compact footprint of only 2 μm × 0.8 μm. Since no conventional electrically driven elements are required to supply power for heating, this device is rather easy to fabricate and has a compact structure. These results show that the device can potentially provide a functionally integrated component for many kinds of efficient all-optical control applications.

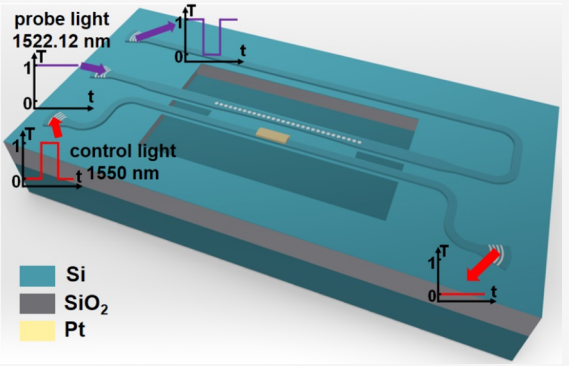


**KEYWORDS:** *thermo-optical effect, photonic crystal nanobeam cavity, photothermal effect, all-optical control*



## 1. INTRODUCTION

Silicon photonics is a promising technology for optical communications, data centers, optical sensing, and high-performance computing due to low propagation loss and latency, high integration, and a CMOS-compatible fabrication process.[1,2] In recent years, silicon photonics is developing rapidly with the breakthroughs of various key integrated photonic devices or systems, such as high-performance optical switches, high-speed electro-optic modulators, broadband optical routers, and an optical computational network.[3−9] Among these various silicon photonic devices, highly energy-efficient tunability is strongly desired. Generally, dynamical control over light propagation in a silicon photonic circuit is usually implemented by shifting the resonance peaks using optical elements such as microrings,[10] microdisks,[11] and photonic crystal cavities[12] to realize switching, modulation, or routing. For the tuning devices that require a large tuning range, thermal-optical tuning is overwhelmingly preferred because of larger refractive index (RI) change, negligible insertion loss, and a much simpler fabrication process.

Highly energy-efficient tunability is desired for thermo-optical tunable resonators, such as on-chip resonator-assisted spectrometers[13] and power-efficient silicon thermo-optic switches with high-speed data rate.[14] Therefore, several approaches have been proposed to improve the heating efficiency, the temporal response, or both.[15−20] Li et al. embedded the p-n junction into the waveguide to directly heat the silicon waveguide and realized a response time of 450 ns and tuning efficiency of 0.12 nm/mW.[16] Zhang et al. improved the tuning efficiency and response time up to 21 nm/mW and ∼68 μs, respectively, based on a suspended photonic crystal nanobeam cavity (PCNC).[18] A thermal tuning efficiency of ∼1.67 nm/mW and a rising time of ∼12.8 μs have been reported based on a silicon microdisk resonator with graphene nanoheaters.[19] However, these devices inevitably suffer from the drawbacks of either low tuning efficiency or large response time. In 2014, Shi et al. demonstrated the all-optical switching using a silicon microdisk resonator integrated with a metal−insulator−metal optical absorber, which, respectively, exhibits a rising and falling time of 2.0 and 2.6 μs.[20] It provides a new method to implement high-efficiency on-chip thermo-optical tuning with response time at the microsecond scale on CMOS-compatible platforms; however, the device shows a tuning efficiency of only 0.255 nm/mW.

In this paper, the all-optical thermo-optic switching is experimentally demonstrated based on a suspended PCNC with an optical heater, which is a metal film placed directly on

Received: September 7, 2021

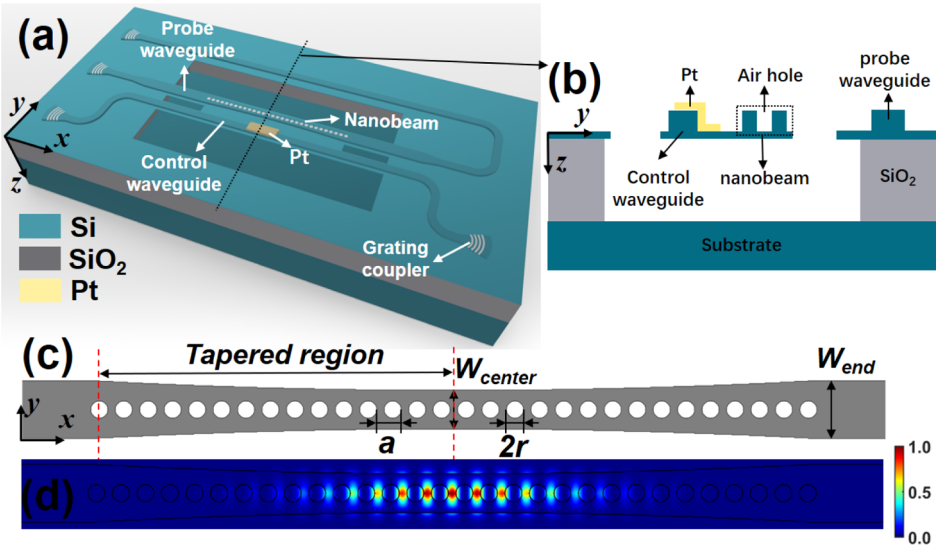


**Figure 1.** (a) 3D view and (b) *yz* cross-section of the suspended thermo-optic switch based on the photothermal effect. (c) Structure and (d) $E_y$ field distribution profile in the *xy* cross-section of the dielectric-mode PCNC.

the top of the ridge waveguide. Due to the suspended waveguide structure, a high tuning efficiency of ~2.79 nm/mW has been demonstrated, which is 10 times higher than that in ref 20, and ~6.8 $\mu$s response time is still at the microsecond time scale. Since no contact electrode pads or oxide isolation layer is required in our device, the fabrication processes are simple. Optical heaters also have a compact structure and can greatly reduce thermal loads and heat leakage compared with the electrical heaters. Additionally, the power supply is only required for the control laser source, and the control signal is transmitted using optical fibers without any electro-optic conversion. Thus, we can remotely control a large number of switching nodes in an all-optical network with low latency. Such photothermal control of light offers the potential for all-optical control in a passive network and all-optical signal processing.

## 2. METHODS

### 2.1. Design of the All-Optical Thermo-Optical Switch.

Figure 1a shows the diagram of the thermo-optic all-optical switch based on a suspended PCNC with a *yz* cross-section shown in Figure 1b. This device consists of a waveguide-coupled PCNC, a probe waveguide, and a control waveguide with a metal film directly deposited on the top. When control light is coupled into the control waveguide and reaches the metal film, it is absorbed and then converted to heat.[20,21] Then, the heat quickly transfers into the PCNC through the silicon slab between the two waveguides. As a result, the RI of silicon increases, and thus, the resonant peaks of the PCNC are red-shifted. Therefore, the all-optical switching can be implemented on the chip.

The silicon-on-insulator (SOI) platform (a 220-nm-thick silicon top layer on a 2-$\mu$m-thick $SiO_2$ layer) is selected to design the device. In our design, A transverse-electric (TE)-polarized dielectric-mode PCNC is utilized since its optical field is concentrated in the silicon region,[22] which enhances the efficiency of the photothermal effect. The slab and ridge thicknesses of the ridge waveguide are 50 and 170 nm, respectively. The period of the PCNC is chosen to be $a$ = 340 nm. The radius of the holes is set to $r$ = 120 nm. As shown in Figure 1c, the number of the air holes on each side is 15. The ridge width of the nanobeam waveguide is quadratically increased from the center width of $W_{center}$ = 540 nm to the width of $W_{end}$ = 800 nm on the both ends. The $E_y$ field distribution profile of the PCNC is calculated by the three-dimensional finite difference time-domain (3D-FDTD) method (Lumerical Solutions, Inc), as shown in Figure 1d. Both the PCNC and the heater structure are suspended to improve the thermal-optic efficiency. The length and width of the air trenches for thermal insulation are 30 and 7 $\mu$m, respectively. We choose platinum (Pt) as the metal absorber of light power because it has excellent chemical stability. Pt can be hardly oxidized in the air when operating at high temperature and also overcome the corrosion during the etching process in a dilute hydrofluoric (HF) acid. Moreover, a Pt film directly deposited on the top of the waveguide can absorb almost all the light in a short distance of less than 2 $\mu$m, which results in an ultra-compact size of the heater. The width, thickness, and length of the Pt film are 0.8 $\mu$m, 100 nm, and 2 $\mu$m, respectively. The control waveguide is 1 $\mu$m away from the probe waveguide with 500 nm ridge width. The distance between the heater and PCNC is set to 0.6 $\mu$m to avoid excess absorption loss from the metal.

Here, we first use FDTD Solutions to calculate the optical power absorption by the metal (Pt) on a waveguide and export it as a heat source. Then, HEAT Solver in DEVICE Solutions (Lumerical Solutions, Inc.) is used to simulate the heating process in the device. The thermal conductivity of silicon, silica, and Pt used in the simulation is set to be 80, 1.38, and 71.6 W/(m·K), respectively. The heat convection coefficient of air is set to be a typical value of 5 W/m$^2$. Figure 2a and b depicts the 3D temperature distribution and *xy* cross-section thermal distribution when the input optical power to the Pt absorber ($P_{abs}$) is 0 mW. It can be seen that the temperature in the center region of the PCNC increases from 300 to ~650 K. In addition, heat is not generated uniformly in Pt and mainly concentrates in the left side since the absorbed optical power decreases exponentially along the propagation direction in the control waveguide.[21] Therefore, we shift the Pt heater to a distance of 0.3 $\mu$m toward the right side in order to make the temperature distribution symmetrical to the center of the


https://doi.org/10.1021/acsphotonics.1c01364
ACS Photonics XXXX, XXX, XXX−XXX

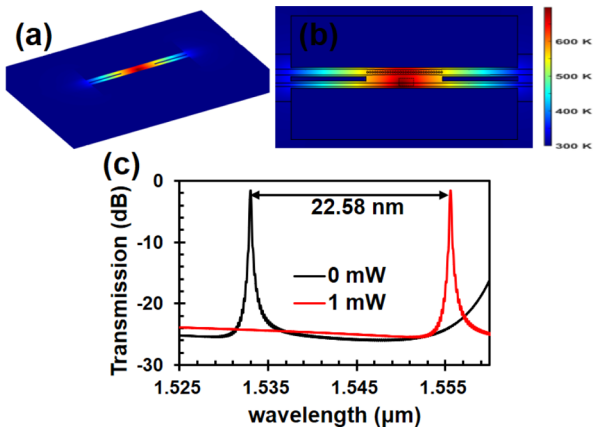


**Figure 2.** (a) 3D temperature distribution and (b) *xy* cross-section thermal distribution of the device. (c) Simulated transmission spectra of the suspended PCNC with different input optical powers $P_{abs}$ of 0 mW and 1 mW, respectively.

PCNC, as shown in Figure 2b. Based on the temperature distribution of the PCNC, we can obtain the RI distribution accordingly. Then, the transmission spectra of the PCNC are calculated using FDTD Solutions, as shown in Figure 2c. It shows a theoretical tuning efficiency of ~22.58 nm/mW.

**2.2. Device Fabrication.** The fabrication processes were started on an SOI wafer with a 220 nm-thick silicon top layer on a 2 $\mu$m-thick $SiO_2$ layer. The ridge waveguides, PCNC, and grating couplers were fabricated with E-beam lithography followed by an ICP-RIE (inductively coupled plasma reactive ion etching) etching. Then, a 100 nm-thick Pt film was sputtered on the control waveguide to realize an optically controlled microheater which has only an extremely small footprint of ~0.8 $\mu$m × 2 $\mu$m. Finally, a dilute HF acid solution was used to remove the oxide layer beneath the PCNC and control waveguide, and then, a free-standing structure was formed. The air trench is only 30 $\mu$m long, so the silicon ridge waveguides are robust enough to avoid deforming. The control and probe lights were coupled into/out from the device through TE-polarized grating couplers. The period and filling factor of the grating couplers are 640 nm and 50%, respectively. The grating couplers were shallowly etched with an etching depth of ~70 nm. The microscope image of the fabricated device is shown in Figure 3a. Figure 3b shows the zoom-in microscope image of the black dashed box in Figure 3a. Figure 3c,d shows the scanning electric microscopy (SEM) images of the central region including the PCNC and heater.

**2.3. Characterization Setup.** Figure 4 shows the setup utilized for the characterization of the fabricated device. The control light and signal light were coupled into the device and detected using a fiber array. The control light (pump light) at 1550 nm was generated using a tunable laser source (Agilent 81640A) and then amplified using an Erbium-doped fiber amplifier. The pumping laser was set to generate the square-wave control light with a frequency of <1 MHz and a duty cycle of 50%. The signal light (probe light) whose wavelength ranges from 1510 to 1640 nm was generated with another tunable laser source (Agilent 81940A). The corresponding output light was detected using a highly sensitive photodetector (Agilent 81618A). The polarization of tunable lasers was controlled to be quasi-TE using polarization controllers.

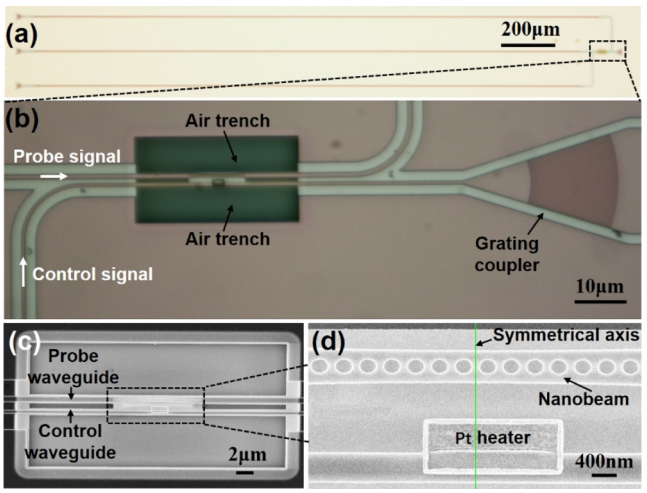


**Figure 3.** (a) Top-view microscope image of the fabricated device. (b) Zoom-in view of the black dashed box in (a). (c) Top-view SEM image of the suspended region. (d) Zoom-in view of the black dashed box in (c).

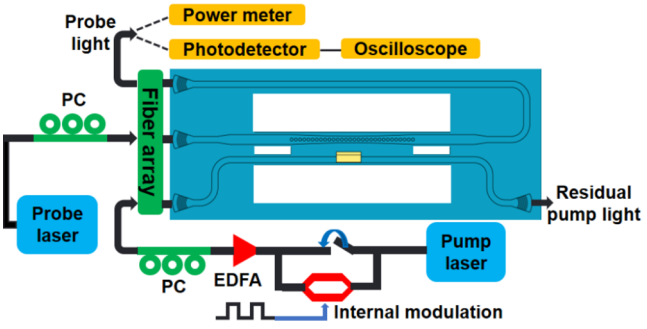


**Figure 4.** Diagram of the experimental setup to characterize the fabricated device.

## 3. RESULTS

The CW pump experiment was conducted for the static characterization of the device. The measured transmission spectra of the PCNC are shown in Figure 5a when different pump powers ($P_{pum}$) are coupled into the device through grating couplers. The spectra have been normalized by the transmission spectrum of a straight ridge waveguide directly connecting a pair of grating couplers. The coupling loss of the TE-polarized grating couplers was measured to be ~7.5 dB/port in the wavelength range from 1530 to 1560 nm, which means $P_{abs} = P_{pum} \times \exp(-7.5/10)$. When no pumping power ($P_{pum}$ = 0 mW) is applied, the resonant wavelength of the fundamental mode, the insertion loss, and the 3dB bandwidth are 1522.12 nm, ~4.1 dB, and 0.21 nm, respectively. When $P_{pum}$ is changed to 6.761 mW, the corresponding resonance peak is red-shifted to 1540.62 nm. Moreover, an extinction ratio of >19 dB for switching can be obtained with only a maximum $P_{pum}$ = 0.716 mW over a 20 nm range. Figure 5b shows the corresponding resonance wavelength shift as a function of $P_{pum}$ and indicates a photothermal efficiency of 15.52 nm/mW. This value is smaller than the theoretical photothermal efficiency of 22.58 nm/mW, which is possibly due to additional loss introduced by the misalignment of the fiber array to the grating couplers or a deviation between the simulated value and the actual value of the thermal conductivities. Such a high photothermal efficiency is enabled


https://doi.org/10.1021/acsphotonics.1c01364
ACS Photonics XXXX, XXX, XXX−XXX

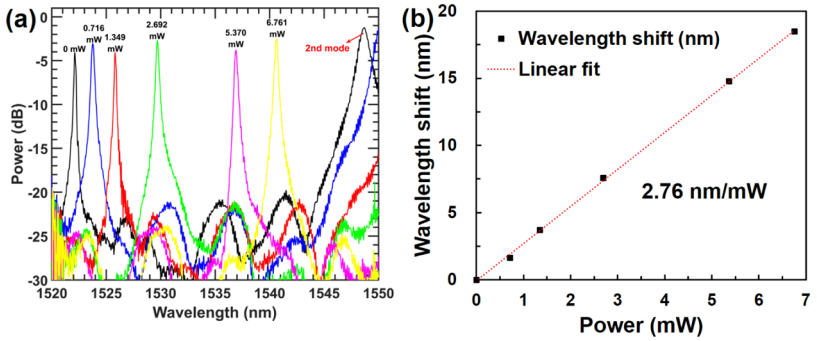


**Figure 5.** (a) Measured transmission spectra of the suspended PCNC with different pumping powers [$P_{pum}$]. (b) Resonance wavelength shifts as a function of different $P_{pum}$s.

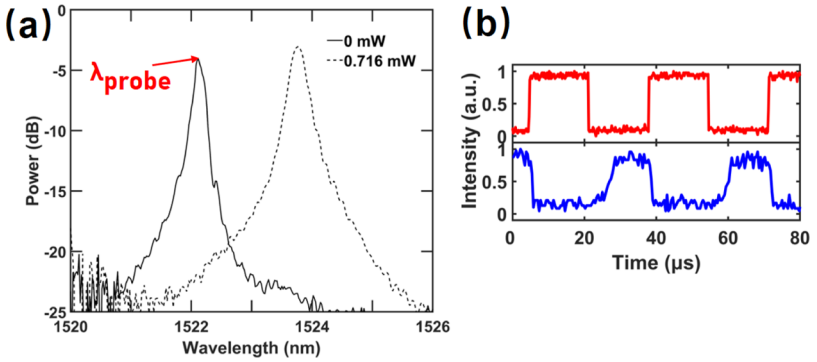


**Figure 6.** (a) Measured spectral responses of the PCNC when $P_{pum}$ = 0 mW (solid line) and $P_{pum}$ = 0.716 mW (dashed line). (b) Measured electrical temporal responses of control pulse (red line) and the corresponding probe output signal (blue line) when probe wavelength is set to $\lambda_{probe}$.

by the novel thermal contact structure and the suspended PCNC design. Note that the resonant wavelength of the second mode is 1548.66 nm when no pump power is applied, so the pump light power $P_{pum}$ for a full-FSR (~26.54 nm) is estimated to be ~10 mW, which indicates the requirement of a quite low $P_{abs}$ of ~ 1.71 mW.

The dynamic response of the switch was measured in the pulsed pump setup by fixing the wavelength of the probe light at $\lambda_{probe}$ = 1522.12 nm and applying a modulated pump light. Here, the pumping laser was set to generate square-wave control light with a frequency of 30 kHz and a duty cycle of 50%. The peak power is 0.716 mW, and thus, the average power of the control light is ~0.358 mW. As shown in Figure 6a, the transmission of the PCNC has a maximal value for the pumping power of 0 mW, while the transmission has the minimum for the pumping power of 0.716 mW. Then, the probe light was modulated by varying the pumping power in this way. Figure 6b shows the dynamic response for the device. The states of "ON" and "OFF" (respectively, corresponds to high and low transmission) of the probe signal output are changed with the control pulse light. The 10−90% rising and falling (corresponds to cooling and heating processes, respectively) times of switching are estimated to be ~6.8 and ~1.6 $\mu$s, respectively. The fall time is much shorter than the rise time. This is because the heater is placed close to the PCNC and can quickly heat the PCNC in the heating process but needs more time to dissipate heat through the long pump and control waveguides at the two sides of the heater in the cooling process. It means that we can obtain faster response by decreasing the length of the air trench or increasing the cross-section of the waveguides at each side of the heater, with the cost of a reduced thermal efficiency.

## 4. DISCUSSION

The proposed device provides a method to realize a switch for all-optical routing, broad-band on-chip optical power meter, and active Q-switcher in low-repetition rate Q-switched lasers. For all-optical routing, we can select the antisymmetric multimode PCNC to realize an add-drop filter.[23,24] In this case, we can add two adiabatic asymmetric directional couplers[25] at the input and output sides of the PCNC to realize an "add-drop" structure similar to multimode-waveguide grating-based filters.[26] Therefore, such an all-optical thermo-optical switch based on the PCNC at the microsecond scale can provide a functionally integrated component for such an ultra-compact and low-power consumption filters. Due to the broadband absorption of metal Pt, the control light can have a large bandwidth. At this point, we can monitor the power variation of control light covering from the telecom band to the mid-infrared band according to the change in the transmission of probe light. Thus, such a device can also provide a functional component for a highly sensitive and broad-band on-chip optical power monitor. This all-optical switch can also be applicable to some low-speed fields like functioning as an active Q-switcher in low-repetition rate Q-switched on-chip lasers. Furthermore, achieving on-chip scalable quantum or cryogenic computing technologies requires photonic integrated circuits to be capable of operation at cryogenic temperatures.[27] Such a highly efficient all-optical switch utilizing the photothermal effect shows advantages over


https://doi.org/10.1021/acsphotonics.1c01364
ACS Photonics XXXX, XXX, XXX−XXX

electric heating in a cryogenic environment due to very small thermal loads and ultra-compact heater.

## 5. CONCLUSIONS

In conclusion, all-optical switching of a silicon PCNC with an ultra-compact heater was experimentally demonstrated based on the photothermal effect. To the best of our knowledge, such a thermo-optic switch has the smallest heater ever reported, with only an ultra-compact footprint of only ∼2 $\mu$m × 0.8 $\mu$m. Consequently, the mechanical strength can be obviously improved with the ultra-compact structure. Meanwhile, a high photothermal tuning efficiency of 15.52 nm/mW is measured due to the novel metal contact and PCNC design on the suspended waveguide structure. The proposed structure also has a relatively fast response time of ∼6.8 $\mu$s, which is comparable to that of the conventional thermal-optical switches based on electrical heaters due to the overall heat capacity of the device. Thus, the proposed all-optical switch based on the PCNC shows the advantages such as ultra-compact size, fast response time, and high photothermal conversion efficiency and compatibility with COMS platforms. This kind of photothermal switch has potential applications such as all-optical control in a passive network and all-optical signal processing.

## AUTHOR INFORMATION


### Corresponding Author

**Yaocheng Shi** − *Center for Optical and Electromagnetic Research, State Key Laboratory for Modern Optical Instrumentation, Zhejiang University, Hangzhou 310058, China*; orcid.org/0000-0003-4489-8310; Email: yaocheng@zju.edu.cn

### Authors

**Penghui Dong** − *Center for Optical and Electromagnetic Research, State Key Laboratory for Modern Optical Instrumentation, Zhejiang University, Hangzhou 310058, China*

**Long Zhang** − *Center for Optical and Electromagnetic Research, State Key Laboratory for Modern Optical Instrumentation, Zhejiang University, Hangzhou 310058, China*

**Daoxin Dai** − *Center for Optical and Electromagnetic Research, State Key Laboratory for Modern Optical Instrumentation, Zhejiang University, Hangzhou 310058, China*

Complete contact information is available at: https://pubs.acs.org/10.1021/acsphotonics.1c01364


### Author Contributions

P.D. and Y.S. conceived the idea. P.D fabricated the devices. P.D. and L.Z. designed and carried out the experiments and performed the data analysis. P.D., Y.S, and D.D. discussed the results. Y.S and D.D. supervised the project. All authors reviewed the manuscript.


### Funding

This work was supported by the National Key Research and Development Program of China (2019YFB2203603), "Pioneer" and "Leading Goose" R&D Program of Zhejiang (2022C01103), and the National Natural Science Foundation of China (6213000026 and 61922070).


### Notes

The authors declare no competing financial interest.

## REFERENCES


(1) Jalali, B.; Fathpour, S. Silicon Photonics. *J. Lightwave Technol.* **2006**, *24*, 4600−4615.
(2) Hochberg, M.; Baehr-Jones, T. Towards fabless silicon photonics. *Nat. Photonics* **2010**, *4*, 492−494.
(3) Xu, Q.; Schmidt, B.; Pradhan, S.; Lipson, M. Micrometre-scale silicon electro-optic modulator. *Nature* **2005**, *435*, 325−327.
(4) Mohsin, M.; Schall, D.; Otto, M.; Noculak, A.; Neumaier, D.; Kurz, H. Graphene based low insertion loss electro-absorption modulator on SOI waveguide. *Opt. Express* **2014**, *22*, 15292−15297.
(5) Almeida, V. R.; Barrios, C. A.; Panepucci, R. R.; Lipson, M.; Foster, M. A.; Ouzounov, D. G.; Gaeta, A. L. All-optical switching on a silicon chip. *Opt. Lett.* **2004**, *29*, 2867−2869.
(6) Yang, L.; Zhou, T.; Jia, H.; Yang, S.; Ding, J.; Fu, X.; Zhang, L. General architectures for on-chip optical space and mode switching. *Optica* **2018**, *5*, 180−187.
(7) Ji, R.; Yang, L.; Zhang, L.; Tian, Y.; Ding, J.; Chen, H.; Lu, Y.; Zhou, P.; Zhu, W. Microring-resonator-based four-port optical router for photonic networks-on-chip. *Opt. Express* **2011**, *19*, 18945−18955.
(8) Yang, L.; Ji, R.; Zhang, L.; Ding, J.; Xu, Q. On-chip CMOS-compatible optical signal processor. *Opt. Express* **2012**, *20*, 13560−13565.
(9) Shen, Y.; Harris, N. C.; Skirlo, S.; Prabhu, M.; Baehr-Jones, T.; Hochberg, M.; Sun, X.; Zhao, S.; Larochelle, H.; Englund, D.; Soljačić, M. Deep learning with coherent nanophotonic circuits. *Nat. Photonics* **2017**, *11*, 441−446.
(10) Zhang, L.; Jie, L.; Zhang, M.; Wang, Y.; Xie, Y.; Shi, Y.; Dai, D. Ultrahigh-Q silicon racetrack resonators. *Photonics Res.* **2020**, *8*, 684−689.
(11) Soltani, M.; Yegnanarayanan, S.; Adibi, A. Ultra-high Q planar silicon microdisk resonators for chip-scale silicon photonics. *Opt. Express* **2007**, *15*, 4694−4704.
(12) Deotare, P. B.; McCutcheon, M. W.; Frank, I. W.; Khan, M.; Lončar, M. High quality factor photonic crystal nanobeam cavities. *Appl. Phys. Lett.* **2009**, *94*, 121106.
(13) Zheng, S. N.; Zou, J.; Cai, H.; Song, J. F.; Chin, L. K.; Liu, P. Y.; Lin, Z. P.; Kwong, D. L.; Liu, A. Q. Microring resonator-assisted Fourier transform spectrometer with enhanced resolution and large bandwidth in single chip solution. *Nat. Commun.* **2019**, *10*, 2349.
(14) Zhang, R.; He, Y.; Zhang, Y.; An, S.; Zhu, Q.; Li, X.; Su, Y. Ultracompact and low-power-consumption silicon thermo-optic switch for high-speed data. *Nanophotonics* **2020**, *10*, 937−945.
(15) Watts, M. R.; Sun, J.; DeRose, C.; Trotter, D. C.; Young, R. W.; Nielson, G. N. Adiabatic thermo-optic Mach-Zehnder switch. *Opt. Lett.* **2013**, *38*, 733−735.
(16) Li, X.; Xu, H.; Xiao, X.; Li, Z.; Yu, Y.; Yu, J. Fast and efficient silicon thermo-optic switching based on reverse breakdown of pn junction. *Opt. Lett.* **2014**, *39*, 751−753.
(17) Dong, P.; Qian, W.; Liang, H.; Shafiiha, R.; Feng, D.; Li, G.; Cunningham, J. E.; Krishnamoorthy, A. V.; Asghari, M. Thermally tunable silicon racetrack resonators with ultralow tuning power. *Opt. Express* **2010**, *18*, 20298−20304.
(18) Zhang, Y.; He, Y.; Zhu, Q.; Guo, X.; Qiu, C.; Su, Y.; Soref, R. Single-resonance silicon nanobeam filter with an ultra-high thermo-optic tuning efficiency over a wide continuous tuning range. *Opt. Lett.* **2018**, *43*, 4518−4521.
(19) Yu, L.; Yin, Y.; Shi, Y.; Dai, D.; He, S. Thermally tunable silicon photonic microdisk resonator with transparent graphene nanoheaters. *Optica* **2016**, *3*, 159−166.
(20) Shi, Y.; Chen, X.; Lou, F.; Chen, Y.; Yan, M.; Wosinski, L.; Qiu, M. All-optical switching of silicon disk resonator based on photothermal effect in metal-insulator-metal absorber. *Opt. Lett.* **2014**, *39*, 4431−4434.
(21) Wu, H.; Ma, K.; Shi, Y.; Wosinski, L.; Dai, D. Ultracompact on-chip photothermal power monitor based on silicon hybrid plasmonic waveguides. *Nanophotonics* **2017**, *6*, 1121−1131.

(22) Quan, Q.; Loncar, M. Deterministic design of wavelength scale, ultra-high Q photonic crystal nanobeam cavities. *Opt. Express* **2011**, *19*, 18529−18542.
(23) Yu, P.; Qiu, H.; Dai, T.; Cheng, R.; Lian, B.; Li, W.; Yu, H. Ultracompact Channel Add-Drop Filter Based on Single Multimode Nanobeam Photonic Crystal Cavity. *J. Lightwave Technol.* **2021**, *39*, 162−166.
(24) Yu, P.; Qiu, H.; Cheng, R.; Chrostowski, L.; Yang, J. High-Q antisymmetric multimode nanobeam photonic crystal cavities in silicon waveguides. *Opt. Express* **2018**, *26*, 26196−26204.
(25) Wang, J.; Xuan, Y.; Qi, M.; Huang, H.; Li, Y.; Li, M.; Chen, X.; Sheng, Z.; Wu, A.; Li, W.; Wang, X.; Zou, S.; Gan, F. Broadband and fabrication-tolerant on-chip scalable mode-division multiplexing based on mode-evolution counter-tapered couplers. *Opt. Lett.* **2015**, *40*, 1956−1959.
(26) Liu, D.; Zhang, M.; Dai, D. Low-loss and low-crosstalk silicon triplexer based on cascaded multimode waveguide gratings. *Opt. Lett.* **2019**, *44*, 1304−1307.
(27) Silverstone, J. W.; Bonneau, D.; O'Brien, J.; Thompson, M. Silicon quantum photonics. *IEEE J. Sel. Top. Quantum Electron.* **2016**, *22*, 6700113.




https://doi.org/10.1021/acsphotonics.1c01364
*ACS Photonics* XXXX, XXX, XXX−XXX